 CMC, vol.9, no.1, pp.25-39, 2009

A Discrete Fourier Transform Framework for Localization Relations

D.T. Fullwood[1], S.R. Kalidindi[2], B.L. Adams[1] and S. Ahmadi[1]

Abstract: Localization relations arise naturally in the formulation of multi-scale models. They facilitate statistical analysis of local phenomena that may contribute to failure related properties. The computational burden of dealing with such relations is high and recent work has focused on spectral methods to provide more efficient models. Issues with the inherent integrations in the framework have led to a tendency towards calibration-based approaches. In this paper a discrete Fourier transform framework is introduced, leading to an extremely efficient basis for the localization relations. Previous issues with the Green's function integrals are resolved, and the method is validated against finite element analysis.

Keywords: Microstructure, crystal structure, elastic behavior, FEM, micromechanical modeling.

1 Introduction

Homogenization relations, linking a material's properties at the mesoscale to those at the macroscale, are fundamental tools for design and analysis of microstructure. Such relations are often achieved through perturbation expansions [Beran (1968), Dederichs and Zeller (1973), Willis (1981), Phan-Thien and Milton (1982)]. Recent advances in this field have successfully applied spectral techniques to Kroner-type perturbation expansions for polycrystalline and composite materials to provide efficient inverse relations for materials design. More recently the same framework has been used to provide 'localization relations' – determination of the local response or its distribution, from a knowledge of the macroscale response employing the same equations used in the calculation of effective properties [Duvvuru, Wu and Kalidindi (2007), Binci, Fullwood and Kalidindi (2008), Kalidindi, Landi and Fullwood (2008)]. The general framework may be applied to a range of material responses with the same basic equations; these include fluid flow, diffusion, elec-

[1] BYU, Provo, UT, U.S.A.
[2] Drexel, Philadelphia, PA, U.S.A

tricity, magnetism and elasticity [Milton (2002)]. In this paper we focus on elasticity, and in particular the local strain as determined from the variation of stiffness in a material; other properties may be analyzed using an analogous route.

Numerical techniques for implementing such homogenization relations have benefited enormously from the application of spectral techniques [Kalidindi, Landi and Fullwood (2008), Adams, Henrie, Henrie, Lyon, Kalidindi and Garmestani (2001), Adams, Kalidindi and Garmestani (2001), Adams, Lyon, Henrie, Kalidindi and Garmestani (2002), Houskamp and Kalidindi (2007), Kalidindi and Duvvuru (2005), Kalidindi, Duvvuru and Knezevic (2006)]. Such methods not only dramatically increase the efficiency of the numerical integrations, but they effectively separate the geometry of the problem from the properties, enabling analysis and optimization of either aspect of the material design to be studied in isolation. Two particular bases used in such spectral frameworks are the primitive basis (see [Adams, Gao and Kalidindi (2005)]) and generalized spherical harmonic functions (GSHF; [Bunge P. R. Morris (1993), Adams (1986)]). The primitive basis provides the benefit of a finite set of functions that are easy to apply and visualize, but lacks the efficiency of the GSHF. In this paper the relations are implemented in a discrete Fourier transform framework that combines advantages of both the primitive and the GSHF bases, while improving the calculation time by orders of magnitude using fast Fourier transforms (FFTs).

When applied to localization methods, analytical techniques, including spectral formulations, have not proven to be accurate, and several studies have resorted to calibration techniques to achieve good results [Duvvuru, Wu and Kalidindi (2007), Binci, Fullwood and Kalidindi (2008), Kalidindi, Landi and Fullwood (2008)]. In order to address the weaknesses in previous models we also tackle several issues not fully addressed in previous spectral frameworks; in particular, the calculation of the Green's function in the region of the central singularity, efficient calculation of the Green's function on a regular grid, and inclusion of the non-zero contribution from the outer surface of the integration volume (for recent work in the area of Green's functions applied to material property relations see [Yang and Tewary (2008)]).

We subsequently demonstrate application of the framework to structures obtained from a pair of isotropic materials, and materials made of polycrystalline components.

2 The Localization Tensor

In keeping with standard notation we will write the stress, strain and displacement within the material as $\boldsymbol{\sigma}$, $\boldsymbol{\varepsilon}$ and $\mathbf{u}$, respectively; the local stiffness tensor is $\mathbf{C}(\mathbf{x})$,

and the reference stiffness tensor for the perturbation analysis is $\mathbf{C}^R$.

We employ an additive decomposition of the strain field in the sample into an average quantity and a perturbation from the average as:

$$\boldsymbol{\varepsilon}(\mathbf{x}) = \bar{\boldsymbol{\varepsilon}} + \boldsymbol{\varepsilon}'(\mathbf{x}), \quad \bar{\boldsymbol{\varepsilon}}' = \mathbf{0} \tag{1}$$

The local perturbation in the strain field can be expressed in terms of a fourth-rank polarization tensor, **a**, as:

$$\boldsymbol{\varepsilon}'(\mathbf{x}) = \mathbf{a}(\mathbf{x})\bar{\boldsymbol{\varepsilon}}, \quad \bar{\mathbf{a}} = \mathbf{0} \tag{2}$$

Then using $\varepsilon_{ij} = (u_{i,j} + u_{j,i})/2$ and $\boldsymbol{\sigma}(\mathbf{x}) = \mathbf{C}(\mathbf{x})\boldsymbol{\varepsilon}(\mathbf{x})$, the conservation principle $\nabla \cdot \boldsymbol{\sigma} = 0$ leads to a differential equation that we may solve using the Green's function method to obtain:

$$\mathrm{a_{klmn}}(\mathbf{x}) = \int_V \frac{1}{2}\left(\mathbf{G}_{\mathrm{ki,l}}\left(\mathbf{x}-\mathbf{x}'\right) + \mathbf{G}_{\mathrm{li,k}}\left(\mathbf{x}-\mathbf{x}'\right)\right) \times \left[\mathbf{C}'_{\mathrm{ijmn}}\left(\mathbf{x}'\right) + \mathbf{C}'_{\mathrm{ijpq}}\left(\mathbf{x}'\right)\ \mathrm{a_{pqmn}}\left(\mathbf{x}'\right)\right]_{,\mathrm{j}} \mathrm{d}\mathbf{x}' \tag{3}$$

where $\mathbf{C}'(\mathbf{x}) = \mathbf{C}(\mathbf{x}) - \mathbf{C}^R$ and G is the Green's function tensor. The value for '**a**' can be repeatedly substituted into the right hand side of the equation to obtain a series that may be written in condensed form as

$$\mathbf{a} = -\boldsymbol{\Gamma}\mathbf{C}' + \boldsymbol{\Gamma}\mathbf{C}'\boldsymbol{\Gamma}\mathbf{C}' - \ldots \tag{4}$$

where $\boldsymbol{\Gamma}$ is the integral operator containing the Green's function. The reason for the alternating sign will become apparent below. For transparency in the development of the theory we will only consider the first term on the right hand side of this equation; the other terms may be handled in a similar manner. Note that the Green's function has a singularity ($\mathrm{G_{ki,l}}(\mathbf{x}-\mathbf{x}') \to \infty$ as $\mathbf{x}-\mathbf{x}' \to 0$), and therefore the integral in Eq. (3) has a principal value in the neighborhood of $\mathbf{x}-\mathbf{x}' = 0$. A common approach to this issue is to evaluate the integral in Eq. (3) using integration by parts over a volume $\tilde{V}$ that lies between two spherical surfaces centered at $\mathbf{x}-\mathbf{x}' = 0$ with radii approaching 0 and ∞, respectively. Considering only the first term

in the series

$$\mathrm{a}_{\mathrm{klmn}}(\mathbf{x}) = -\boldsymbol{\Gamma}\mathbf{C}'$$

$$= \left[\int_S \frac{1}{2}\left(\mathrm{G}_{\mathrm{ki,l}}\left(\mathbf{x}-\mathbf{x}'\right)+\mathrm{G}_{\mathrm{li,k}}\left(\mathbf{x}-\mathbf{x}'\right)\right)\left[\mathbf{C}'_{\mathrm{ijmn}}\left(\mathbf{x}'\right)\right] n_j \mathrm{d}S\right]_{\substack{\text{sphere with}\\ |\mathbf{x}-\mathbf{x}'|\to\infty}}^{\substack{\text{sphere with}\\ |\mathbf{x}-\mathbf{x}'|\to 0}}$$

$$-\int_{\tilde{V}} \frac{1}{2}\left(\mathrm{G}_{\mathrm{ki,lj}}\left(\mathbf{x}-\mathbf{x}'\right)+\mathrm{G}_{\mathrm{li,kj}}\left(\mathbf{x}-\mathbf{x}'\right)\right)\left[\mathbf{C}'_{\mathrm{ijmn}}\left(\mathbf{x}'\right)\right]\mathrm{d}\mathbf{x}' \quad (5)$$

Of the two spherical surface integrals in the first term of Eq. (5) the second integral corresponding to $\mathbf{x}-\mathbf{x}' \to 0$ is the principal value term. Clearly when $\mathbf{x} \approx \mathbf{x}'$ on the surface of this infinitesimal sphere, $\mathbf{C}'_{\mathrm{ijmn}}(\mathbf{x}') = \mathbf{C}'_{\mathrm{ijmn}}(\mathbf{x})$, which is a constant, and can be taken outside of the integral. Combine the integrands into tensors:

$$\begin{aligned}
E_{klij} &= \lim_{|\mathbf{x}-\mathbf{x}'|\to 0}\left(\int_S \frac{1}{2}\left(\mathrm{G}_{\mathrm{ki,l}}\left(\mathbf{x}-\mathbf{x}'\right)+\mathrm{G}_{\mathrm{li,k}}\left(\mathbf{x}-\mathbf{x}'\right)\right) n_j \mathrm{d}S\right)\\
I^{\infty}_{klij} &= \lim_{|\mathbf{x}-\mathbf{x}'|\to\infty}\left(\int_S \frac{1}{2}\left(\mathrm{G}_{\mathrm{ki,l}}\left(\mathbf{x}-\mathbf{x}'\right)+\mathrm{G}_{\mathrm{li,k}}\left(\mathbf{x}-\mathbf{x}'\right)\right)\left[\mathbf{C}'_{\mathrm{ijmn}}\left(\mathbf{x}'\right)\right] n_j \mathrm{d}S\right)\\
\Phi_{klij}\left(\mathbf{x}-\mathbf{x}'\right) &= \frac{1}{2}\left(\mathrm{G}_{\mathrm{ki,lj}}\left(\mathbf{x}-\mathbf{x}'\right)+\mathrm{G}_{\mathrm{li,kj}}\left(\mathbf{x}-\mathbf{x}'\right)\right)
\end{aligned} \quad (6)$$

The term I^{∞}_{klij} is typically assumed to equal zero, however this assumption is generally not valid. This is easy to see if we take an isotropic reference tensor and the resultant analytical values of $\mathrm{G}_{\mathrm{ki,l}}$. Suppose that the isotropic stiffness tensor has Lamé constants λ, μ and that $\mathbf{x}-\mathbf{x}' = \mathbf{r}$.

$$\mathrm{G}_{\mathrm{ki,l}}(\mathbf{r}) = \frac{1}{8\pi\mu(\lambda+2\mu)}\left\{\frac{(\lambda+\mu)\left(\delta_{kl}r_i+\delta_{il}r_k\right)-(\lambda+3\mu)\,\delta_{ki}r_l}{|r|^3} - \frac{3(\lambda+\mu)\,r_i r_k r_l}{|r|^5}\right\} \quad (7)$$

Since this is proportional to $1/|r|^2$ the integral over the surface of a sphere remains approximately constant. In fact if the stiffness tensor is constant throughout the material (and hence can be taken outside the integral), then clearly the integral over the outer sphere is simply the negative of the integral over the inner sphere. If we

make the common assumption that the material is random at infinity (completely uncorrelated) then the stiffness tensor on a patch of the outer sphere is approximately $\overline{\mathbf{C}'}$ - the average value of the perturbation stiffness. Then the integral on the outer sphere may be approximated by

$$I^{\infty} \approx \mathbf{E}\overline{\mathbf{C}'} \tag{8}$$

Hence we may rewrite Eq. (5) as:

$$\mathbf{a}(\mathbf{x}) = \mathbf{E}\overline{\mathbf{C}'} - \mathbf{E}\mathbf{C}'(\mathbf{x}) - \int_{\tilde{V}} \mathbf{\Phi}\left(\mathbf{x}-\mathbf{x}'\right)\mathbf{C}'\left(\mathbf{x}'\right)\mathrm{d}\mathbf{x}' \tag{9}$$

Clearly if $\mathbf{C}^R = \bar{\mathbf{C}}$ then $\overline{\mathbf{C}'} = \mathbf{0}$ and $\mathbf{E}^{\infty}$ as calculated from Eq. (8) tends to zero, in which case we arrive at the more common first-order form of the localization equation

$$a_{klmn}(\mathbf{x}) = -\mathrm{E}_{\mathrm{klij}}\mathbf{C}'_{\mathrm{ijmn}}(\mathbf{x}) - \int_{\tilde{V}} \Phi_{\mathrm{klij}}\left(\mathbf{x}-\mathbf{x}'\right)\mathbf{C}'_{\mathrm{ijmn}}\left(\mathbf{x}'\right)\mathrm{d}\mathbf{x}' \tag{10}$$

In general we will not restrict the reference tensor to equal the average stiffness tensor, hence we will use Eq. (9) rather than Eq. (10).

For completeness we repeat the commonly known definitions of $\mathbf{E}$ and $\mathbf{\Phi}$ for an isotropic reference tensor:

$$E_{\mathrm{ijkl}} = \frac{1}{15\mu}\left\{\frac{\lambda+\mu}{\lambda+2\mu}\delta_{ij}\delta_{kl} - \frac{3\lambda+8\mu}{\lambda+2\mu}I_{ijkl}\right\} \tag{11}$$

where $\mathbf{I}$ is the fourth order symmetrized tensor identity:

$$I_{ijkl} = \frac{1}{2}\left(\delta_{ik}\delta_{jl} + \delta_{il}\delta_{jk}\right) \tag{12}$$

$$\begin{aligned}\Phi_{ijkl} = {} & \frac{1}{8\pi\mu(\lambda+2\mu)r^3}\times \\ & \Big[(\lambda+\mu)\left(\delta_{ij}\delta_{kl} - 3\delta_{ij}n_kn_l - 3\delta_{kl}n_in_j + 15n_in_jn_kn_l\right) - \mu\left(\delta_{ik}\delta_{jl} + \delta_{il}\delta_{jk}\right) \\ & - 3\lambda\left(\delta_{ik}n_jn_l + \delta_{il}n_jn_k + \delta_{jk}n_in_l + \delta_{jl}n_in_k\right)/2\Big]\end{aligned} \tag{13}$$

where $\mathbf{n}=\mathbf{r}/|\mathbf{r}|$.

3 Spectral Form

Consider the formula for localization tensor as given in Eq. (9). Equations of this type have benefited from rewriting in spectral form in various previous studies [Binci, Fullwood and Kalidindi (2008), Kalidindi, Landi and Fullwood (2008)]. One benefit of a spectral formulation is the ability to split material data from structure data for efficient design studies. Another immediate benefit may be seen in the calculation of the final term of the equation. The convolution can be efficiently calculated using fast Fourier transforms if the data is in discrete form. Let us combine the $\mathbf{E}$ and $\mathbf{\Phi}$ terms into a single term, $\mathbf{\Gamma}$ as in Eq. (5). Discretize the values of this integrand on a regular grid as follows (normalized to remove the requirement for an extra normalization term on the integrals):

$$\mathbf{\Gamma}(\mathbf{r}) \approx \frac{1}{\delta^3}\mathbf{\Gamma}_t \chi_t(\mathbf{r}), \quad \mathbf{\Gamma}_t = \int_{R(\Omega)} \mathbf{\Gamma}(\mathbf{r})\,\chi_t(\mathbf{r})\,d\mathbf{r} \tag{14}$$

where $\chi_t(\mathbf{r})$ is the indicator function for the spatial cell around discrete point $\mathbf{r}_t$, taking the value 1 for vectors lying in the cell, and 0 for vectors lying outside of it; and δ^3 is the volume of one of these uniformly sized cells. If values of $\mathbf{x}$ are defined on a discrete grid (obviously of the same spacing as $\mathbf{r}$) and enumerated by s, then a discrete form of the localization tensor can be defined:

$$\mathbf{a}_s = -\sum_t \mathbf{\Gamma}_t \mathbf{C}'_{s-t} \tag{15}$$

In the evaluation of $\mathbf{\Gamma}_t$ using Eq. (14) special care must be taken in the vicinity of the origin due to the singularity. The main issue here is calculation of the integral of Φ in the cell about the origin $\mathbf{r}$=$\mathbf{0}$. Various previous studies have either ignored the integral of Φ in the central cell, assuming that it was negligible, or have evaluated it using a regular grid of integration points. Accurate calculations using Monte-Carlo integration have established that the value of the integral in the central cell accounts for approximately 15% of the total Φ integral; and this is almost independent of the size of the cell. To qualify this last statement, we mean that the value of the integral is independent of the size of the central cell if there is only a single material state within the cell. We illustrate this issue in Fig. 1. Suppose that we numerically integrate at rectangular grid points in a cell about the origin (shown as the open circle in the figures to emphasize that we must avoid integrating at the singularity). Since the integral of Φ between two cubes is zero, refining the grid, or including points closer to the origin (as in Fig. 1b) will not improve the accuracy. We need to integrate the white area outside the central circle to determine the main contribution from Φ in this cell. For the results in this paper this was done to high accuracy using Monte-Caro integration for each of the reference tensors used in the calculations [Caflisch (1998)].

It is worth noting that an equivalent approach would be to calculate E on the surface of a cube about the origin rather than on a sphere. In this case the calculation for Φ in the inner cell would be zero (since it would be over a volume between two cubes), and the correction from previous work would be carried by the new value of $\mathbf{E}$. This method was also tested as an alternative to that mentioned above. Since there is no known analytical solution for the calculation of $\mathbf{E}$ on the surface of a cube a Monte-Carlo integration was again employed, thus giving no significant advantage to the alternative.

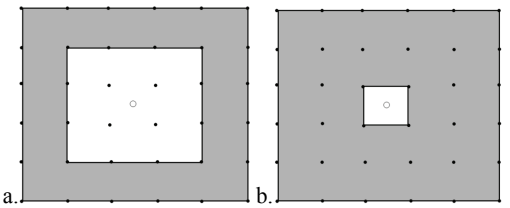

Figure 1: Schematic of an integration region (grey) about the origin (open circle) that is not improved by taking extra points on the grid about the origin (b.)

For calculation of values of $\mathbf{\Gamma}_t$ at values of t other than zero, clearly the value of Φ decreases rapidly with distance from the origin, hence one may use a decreasing grid refinement and maintain the same accuracy. The most efficient grid spacing for the numerical integration in these cells was found to be for an odd number of points in each direction, centered about the origin of the cell, and with spacings i/p from the origin (in a unit cell; i indicates integer values, and p are the number of points in each direction).

Adjustments of the integral to include the region between the rectangular region over which we wish to take the FFTs, and the 'infinite' sphere over which the Green's function is calculated was demonstrated in a previous paper [Kalidindi, Binci, Fullwood and Adams (2006)]. As an example of the contribution made to the overall integral from the different regions we graph the magnitudes for an example case of a material constructed of two isotropic media in Fig. 2. While the principal value term (the integral on the inner spherical surface) is dominant, all terms are significant, and cannot be ignored.

We wish to separate the material data from the structure data in our formulation for the localization tensor. Hence we introduce a convenient function for holding the structure information [Adams, Gao and Kalidindi (2005)]; the microstructure function $m(\mathbf{x},h)$ is a distribution function on the local state space for each point in

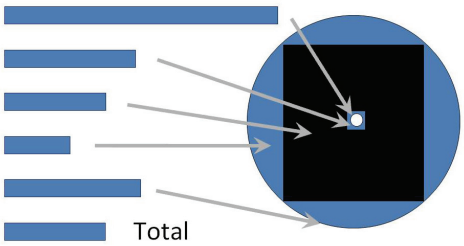

Figure 2: Absolute values of contributions from different terms of the Green's function integrals (from the inside to the outside of the integration region) shown as bars, for an example material of two isotropic media. A bar representing the total integral is also shown. The black region indicates the volume that is integrated directly using a rectangular (FFT) grid.

the RVE:

$$\int_a^b m(\mathbf{x},h)dh = P(a \leq h(\mathbf{x}) \leq b) \tag{16}$$

This is sometimes written in the alternative manner involving the infinitesimal neighborhood, V, of the point $\mathbf{x}$:

$$m(\mathbf{x},h)\,dh = \frac{dV_h}{V} = f(h)|_{\mathbf{x}} dh \tag{17}$$

where dV_h represents the volume of material in volume element V that is in a state that lies in a neighborhood dh of h. Such a description allows for a continuous state space (such as orientation), but also permits multiple states to exist at a single 'point' of the sample.

The motivation for this definition stems from the fact that material information is generally derived from data gathered in a neighborhood rather than a single point. This is obvious for a local state such as orientation, which is in fact defined in terms of relative positions of atoms in a neighborhood; but it is also true that instruments gather information from an area or volume determined by their resolution rather than from a single point. We wish to discretize the function $m(\mathbf{x},h)$ in both the real space, $\Re^n$, and the local state space, H. This is consistent with many characterization techniques that read data from a discrete grid of the material sample. As before, the real space is discretized into a regular grid, with vertices enumerated by s=1:S, and the local state space is enumerated by n=1:N. We will write $m_s^n = m(\mathbf{x}_s, h_n)$.

Then we may write $\mathbf{C}'_{s-t} = \sum_n \mathbf{C}'^n m^n_{s-t}$. And

$$\mathbf{a}_s = \sum_t \mathbf{\Gamma}_t \sum_n \mathbf{C}'^n m^n_{s-t} \tag{18}$$

Taking the Fourier transforms of both sides and using Plancherel's theorem and the convolution theorem

$$\mathbf{A}_k = \frac{1}{N} \sum_{j=1:N} \tilde{\Gamma}_k \left(\tilde{C}^j\right)^* M^j_k \tag{19}$$

where $\tilde{C}^j$ is the FFT of $\mathbf{C}'^n$, $\tilde{\Gamma}_k$ is the FFT of $\mathbf{\Gamma}_t$, and $M^j_k = \Im_s\left(\Im_n\left(m^n_s\right)\right)$; $\Im_n$ indicates FFT with respect to variable n, and the asterisk indicates complex conjugation. We may combine the first two terms on the right side of the equation to give

$$\mathbf{A}_k = \frac{1}{N} \sum_{j=1:N} Z^j_k M^j_k \tag{20}$$

Thus we have effectively split the structural information of the material contained in the microstructure function from the property information contained in the local stiffness tensor. This is a very efficient way to calculate the localization tensor for each point in the material. Not only does it dramatically cut down the number of operations involved in the original convolution (in the spatial dimensions), but it also enables compression of the data. In Fourier space the most significant terms in the series are generally gathered at the start of the series; one may often ignore higher order terms with minimal loss in accuracy. This is the basis for compression techniques such as those used in the imaging and sound industries. Hence one may ignore the majority of the terms in $\tilde{C}^j$ with little influence on the accuracy (see the examples below). This approach dramatically reduces the summation in Eq. (20), leading to even higher efficiency. Since these terms are only calculated once for a given reference tensor, the significant terms may be stored in a concise database for economical material analysis and design. For localization calculations the higher order terms of $\tilde{\Gamma}_k$ may not necessarily be ignored, as such 'smoothing' would significantly reduce the accuracy at individual points. Hence there is likely to be little compression in the spatial dimensions in Fourier space. However, for effective property calculations (which are not considered in this paper) it may be possible to gain compression in the spatial dimensions without significant loss of accuracy.

One consequence of the use of FFTs to calculate the convolution in Eq. (18) is the introduction of periodic boundary conditions. While different boundary conditions may be utilized by padding in the various dimensions [Fullwood, Kalidindi,

Niezgoda, Fast and Hampson (2008)], periodic boundaries were assumed for this paper. Since the integral is centered at the origin (about **x**), the vectors represented by t in Eq. (18) have a maximum length in each dimension of half the size of the sample, in order to represent a cube that is centered at the origin, and of the same side dimensions as the sample. Care must be taken in setting up the relevant tensors to reflect this. Note also that the calculations are expedited by writing the stiffness tensors in 9x9 matrix form.

4 Applications: Local Strains and Strain Distributions

In order to test the validity of the formulation given above various material structures were evaluated using finite element analysis to determine the local strains based upon an applied global strain. The results were compared with calculations using the method outlined above. A hypothetical material was constructed of two isotropic phases of varying contrast in their stiffness coefficients. For these tests the reference tensor was assumed to be given by the mean of that for the two constituents, independent of the overall volume fractions of these constituents.

Example structures are shown in Fig. 3 for 75% of the stiff phase. The structures are randomly dispersed single cells, unidirectional fibers and laminates. The Lamé constants for the two materials are $\mu = 35, \lambda = 75$ and $\mu = 55, \lambda = 100$ respectively; a global strain of 1% was applied in the 3-direction. The average relative error between the FEM results and the analytical framework is 4.2% (for recent work on homogenization using FEM see [Xu, Fan, Xie and Li (2008)]). A plot of strain vs cell number for the analytical (dotted) and FE (solid) results is shown in Fig. 4. The analytical results correlate well with the FEM calculations.

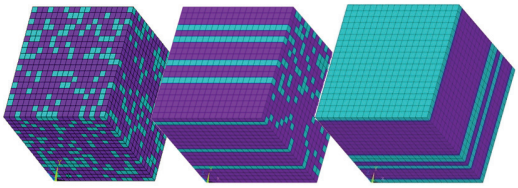

Figure 3: Schematic of 2-phase cube with darker areas representing stiffer phase (75% volume fraction) for a. random, b. fiber and c. laminate structures.

In this example the reference tensor was chosen to be the mean of the two isotropic constituents, and not the average stiffness tensor. This choice highlights the importance of the first term on the right hand side of Eq. (10). Without this term the average strain as calculated by the spectral method was 4% different from the

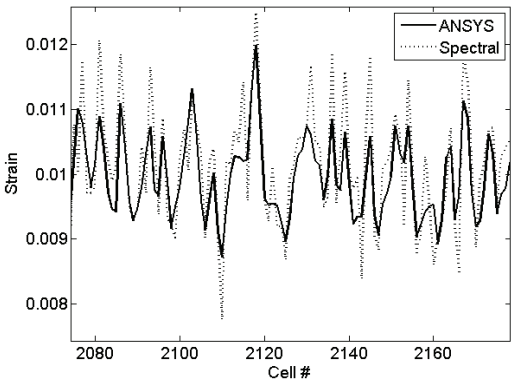

Figure 4: Typical graph of strain vs cell number as calculated by the spectral method (dotted) vs finite element (solid). A macroscopic strain of 1% is applied to the cube of Fig. 3a in the z-direction.

applied (macro) strain; with this term the difference was less than 0.2%. The differences would be more apparent with phases of higher contrast. The ability to choose a reference tensor that is not the mean of the constituent tensors is critical to efficient material design. If the calculations use the mean tensor, then the Green's function terms in the integrals must be re-evaluated for each choice of material structure (since the mean would change). A better choice is to choose a reference tensor that lies between the stiffness tensors of the constituent phases [Kalidindi, Binci, Fullwood and Adams (2006)]. Then only the values of M_k^j change in Eq. (20), leading to rapid optimization / analysis of material design.

Of significance in many failure calculations is the probability of local high stresses or strains due to the geometrical interrelations of the material constituents. This information is captured in the stress or strain distribution for the material. Figure 5 shows the strain distribution as calculated by FEM and using the spectral method for a variety of structures. The distributions for the strains in the two material components are given. The spectral method reasonably captures the shapes of the distributions. For each structure the average error in calculated strain is less than 5%.

In order to test the potential compression of terms in the material database from using spectral form, local strain in a copper polycrystal was considered. The lattice orientation was assumed to be governed by a single axis of rotation (the $\mathbf{e}_1$ axis), with the local state being determined by a rotation, θ, about this axis; this simplified description enabled the study to be carried out over a single dimension,

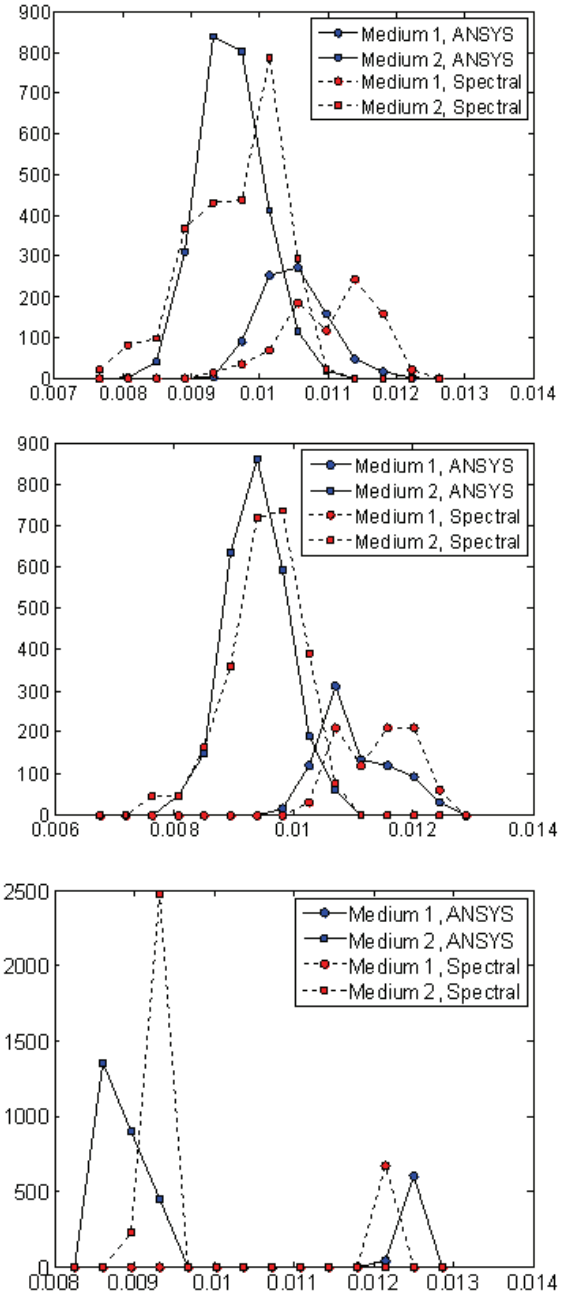

Figure 5: Strain distributions for the stiff (square markers) and soft (circle markers) phases of various structures as calculated by the new spectral method (dashed) vs finite element (solid). A 1% macroscopic strain is applied to the cubes in the z-direction (perpendicular to the laminates).

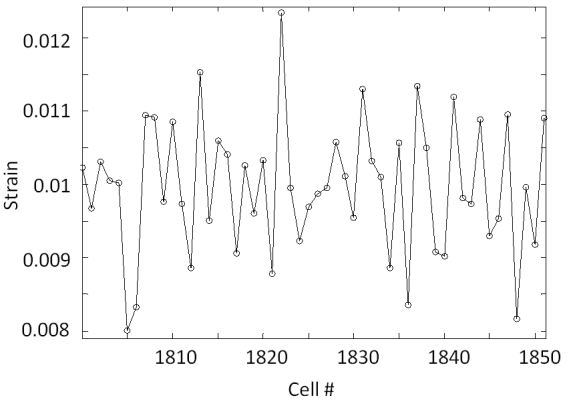

Figure 6: Strain as calculated using the full material data in Fourier space (black line) and using only 3% of the data (circles). The error is less than 1%.

given by θ. A method for incorporating all 3 Euler angles of lattice orientation into the spectral framework will be discussed in future work. The calculation was performed with 97% of the $\tilde{C}^j$ terms in Eq. (19) being ignored. The result was a negligible difference in the calculated strain (Fig. 6). As noted in the previous section, the compression resulting from the FFTs is in the orientation dimension, and not in the spatial dimension for these localization relations.

5 Conclusions

A spectral framework based upon discrete Fourier transforms has been developed for localization relations, providing an efficient framework for analysis and design of materials. The framework has been validated against finite element calculations, and results in good accuracy for materials with low contrast in properties between the phases. The contrast between the stiffness tensors of phases used in the examples of this paper are similar to the contrast found in a single phase polycrystal metal or ceramic. Higher order terms of the series expansion could be included into the framework to improve accuracy for higher contrast examples. These might include, for example, fiber reinforced composites.

Several issues regarding the integration of the Green's function have been addressed during the development of the method, resulting in significant improvements in accuracy when a rectangular grid is used as the basis for the integration.

Acknowledgement: This work was partially supported by the ARO, program

manager, David Stepp.

References

Adams, B. L. (1986): Description of the intercrystalline structure distribution in polycrstaline materials, *Metallurgical Transactions A (Physical Metallurgy and Materials Science)*, 17A, 12, 2199-2207.

Adams, B. L., Gao, X., Kalidindi, S. R. (2005): Finite approximations to the second-order properties closure in single phase polycrystals, *Acta Materialia*, 53, 13, 3563-3577.

Adams, B. L., Henrie, A., Henrie, B., Lyon, M., Kalidindi, S. R., Garmestani, H. (2001): Microstructure-sensitive design of a compliant beam, *Journal of the Mechanics and Physics of Solids*, 49, 8, 1639-1663.

Adams, B. L., Kalidindi, S. R., Garmestani, H. (2001): *Spectral representation of microstructure evolution in polycrystals*, Minerals, Metals and Materials Society, 67-72.

Adams, B. L., Lyon, M., Henrie, B., Kalidindi, S. R., Garmestani, H. (2002): Spectral integration of microstructure and design, *Materials Science Forum*, 408-412, 487-492.

Beran, M. J. (1968): *Statistical continuum theories*, NY:John Wiley Interscience.

Binci, M., Fullwood, D., Kalidindi, S. R. (2008): A new spectral framework for establishing localization relationships for elastic behavior of composites and their calibration to finite-element models, *Acta Materialia*, 56, 10, 2272-2282.

Bunge, H.-J. (1993): *Texture analysis in materials science. Mathematical Methods*, Cuvillier Verlag.

Caflisch, R. E. (1998): Monte Carlo and quasi-Monte Carlo methods, *Acta Numerica*, 7, 1-49.

Dederichs, P. H., Zeller, R. (1973): Variational treatment of the elastic constants of disordered materials, *Z. Physik A*, 259, 103-116.

Duvvuru, H. K., Wu, X., Kalidindi, S. R. (2007): Calibration of elastic localization tensors to finite element models: Application to cubic polycrystals, *Computational Materials Science*, 41, 2, 138-144.

Fullwood, D. T., Kalidindi, S. R., Niezgoda, S. R., Fast, T., Hampson, N. (2008): Gradient-based Microstructure Reconstructions from Distributions Using Fast Fourier Transforms, *Materials Science & Engineering A*, 494, 68-72.

Houskamp, J., Kalidindi, S. R. (2007): Application of the Spectral Methods of Microstructure Design to Continuous Fiber Reinforced Composites, *Journal of*

Composite Materials, 41, 909.

Kalidindi, S. R., Duvvuru, H. K. (2005): Spectral methods for capturing crystallographic texture evolution during large plastic strains in metals, *Acta Materialia*, 53, 13, 3613-3623.

Kalidindi, S. R., Duvvuru, H. K., Knezevic, M. (2006): Spectral calibration of crystal plasticity models, *Acta Materialia*, 54, 7, 1795-1804.

Kalidindi, S. R., Landi, G., Fullwood, D. T. (2008): Spectral representation of higher-order localization relationships for elastic behavior of polycrystalline cubic materials, *Acta Materialia*, 56, 15, 3843-3853.

Kalidindi, S. R., Binci, M., Fullwood, D., Adams, B. L. (2006): Elastic properties closures using second-order homogenization theories: Case studies in composites of two isotropic constituents, *Acta Materialia*, 54, 11, 3117-3126.

Milton, G. W. (2002): *The Theory of Composites*, Cambridge University Press.

Phan-Thien, N., Milton, G. W. (1982): New bounds on effective thermal conductivity of n-phase materials, *Proc. R. Soc. London A*, 380, 333-348.

Willis, J. R. (1981): Variational and related methods for the overall properties of composites, *Adv. Appl. Mech.*, 21, 1-78.

Xu, L. M., Fan, H., Xie, X. M., Li, C. (2008): Effective elastic property estimation for bi-continuous heterogeneous solids, *CMC: Computers, Materials & Continua*, Vol. 7, No. 3, 119-127.

Yang, B., Tewary, V. K. (2008): Green's function for multilayers with interfacial membrane and flexural rigidities, *CMC: Computers, Materials & Continua*, Vol. 8, No. 1, 23-31.